Supplement of Atmos. Chem. Phys., 18, 8491–8504, 2018
https://doi.org/10.5194/acp-18-8491-2018-supplement

Atmospheric Chemistry and Physics
Open Access
EGU

Supplement of

Widespread air pollutants of the North China Plain during the Asian summer monsoon season: a case study

Jiarui Wu et al.

Correspondence to: Guohui Li (ligh@ieecas.cn) and Junji Cao (jjcao@ieecas.cn)

Supplement

The supplement provides description about the WRF-CHEM model configuration, methodology, synoptic conditions, model evaluations and the effect of interaction between NCP and non-NCP emissions during the study episode.

Section S1 WRF-CHEM Model and Configuration

S1.1 WRF-CHEM Model

The WRF-CHEM used in this study includes a new flexible gas phase chemical module and the CMAQ aerosol module developed by US EPA (Li et al., 2010; Binkowski and Roselle, 2003). In this aerosol component, the particle size distribution is represented as the superposition of three lognormal sub-distributions, called modes. The processes of coagulation, particles growth by the addition of mass, and new particle formation are included. The wet deposition employs the method used in the CMAQ and the surface deposition of chemical species is parameterized following Wesely (1989). The photolysis rates are calculated using the FTUV (Li et al., 2005, 2011a, b), considering the effects of aerosols and clouds on photolysis.

S1.2 Model Configuration

The physical parameterizations include the microphysics scheme of Hong et al (Hong and Lim, 2006), the Mellor, Yamada, and Janjic (MYJ) turbulent kinetic energy (TKE) planetary boundary layer scheme (Janjić, 2002), the Unified Noah land-surface model (Chen and Dudhia, 2001), the Goddard longwave radiation scheme (Chou and Suarez, 2001) and the Goddard shortwave parameterization (Chou and Suarez, 1999). The NCEP 1° × 1° reanalysis data are used to obtain the meteorological initial and boundary conditions, and the meteorology has been nudged in the model simulation. The chemical initial and boundary conditions are interpolated from the 6h output of MOZART (Horowitz et al., 2003). The

spin-up time of the WRF-CHEM model is 28 hours. The SAPRC-99 (Statewide Air Pollution Research Center, version 1999) chemical mechanism is used in the present study. The anthropogenic emissions are developed by Zhang et al. (2009), including contributions from agriculture, industry, power generation, residential, and transportation sources. The biogenic emissions are calculated online using the MEGAN (Model of Emissions of Gases and Aerosol from Nature) model developed by Guenther et al (2006).

Section S2 Methodology

S2.1 Factor Separation Approach

The formation of the secondary atmospheric pollutant, such as O_3, secondary organic aerosol, and nitrate, is a complicated nonlinear process in which its precursors from various emission sources and transport react chemically or reach equilibrium thermodynamically. Nevertheless, it is not straightforward to evaluate the contributions from different factors in a nonlinear process. The factor separation approach (FSA) proposed by Stein and Alpert (1993) can be used to isolate the effect of one single factor from a nonlinear process and has been widely used to evaluate source effects (Gabusi et al., 2008; Weinroth et al., 2008; Carnevale et al., 2010; Li et al., 2014a; Wu et al., 2017). The total effect of one factor in the presence of others can be decomposed into contributions from the factor and that from the interactions of all those factors.

Suppose that field $\boldsymbol{f}$ depends on a factor $\boldsymbol{\varphi}$:

$$\boldsymbol{f} = \boldsymbol{f}(\boldsymbol{\varphi})$$

The FSA decomposes function $\boldsymbol{f}(\boldsymbol{\varphi})$ into a constant part that does not depend on $\boldsymbol{\varphi}$ $(\boldsymbol{f}(\mathbf{0}))$ and a $\boldsymbol{\varphi}$-depending component $(\boldsymbol{f}'(\boldsymbol{\varphi}))$, as follows:

$$\boldsymbol{f}'(\mathbf{0}) = \boldsymbol{f}(\mathbf{0})$$

$$\boldsymbol{f}'(\boldsymbol{\varphi}) = \boldsymbol{f}(\boldsymbol{\varphi}) - \boldsymbol{f}(\mathbf{0})$$

Considering that there are two factors *X* and *Y* that influence the formation of secondary pollutants in the atmosphere and also interact with each other. Denoting $\boldsymbol{f_{XY}}$, $\boldsymbol{f_X}$, $\boldsymbol{f_Y}$, and $\boldsymbol{f_0}$ as the simulations including both of two factors, factor *X* only, factor *Y* only, and none of the two factors, respectively. The contributions of factor *X* and *Y* can be isolated as follows:

$$\boldsymbol{f'_X = f_X - f_0}$$

$$\boldsymbol{f'_Y = f_Y - f_0}$$

Note that term $\boldsymbol{f'_{X(Y)}}$ represents the impacts of factor *X(Y)*, while $\boldsymbol{f_0}$ is the term independent of factors *X* and *Y*.

The simulation including both factors *X* and *Y* is given by:

$$\boldsymbol{f_{XY} = f_0 + f'_X + f'_Y + f'_{XY}}$$

The mutual interaction between *X* and *Y* can be expressed as:

$$\boldsymbol{f'_{XY} = f_{XY} - f_0 - f'_X - f'_Y = f_{XY} - (f_X - f_0) - (f_Y - f_0) - f_0 = f_{XY} - f_X - f_Y + f_0}$$

The above equation shows that the study needs four simulations, $\boldsymbol{f_{XY}, f_X, f_Y}$ and $\boldsymbol{f_0}$, to evaluate the contributions of two factors and their synergistic interactions.

S2.2 Statistical metrics for observation-model comparisons

In the present study, the mean bias (*MB*), root mean square error (*RMSE*) and the index of agreement (*IOA*) are used as indicators to evaluate the performance of WRF-CHEM model in simulation against measurements. *IOA* describes the relative difference between the model and observation, ranging from 0 to 1, with 1 indicating perfect agreement.

$$\boldsymbol{MB = \frac{1}{N}\sum_{i=1}^{N}(P_i - O_i)}$$

$$\boldsymbol{RMSE = \left[\frac{1}{N}\sum_{i=1}^{N}(P_i - O_i)^2\right]^{\frac{1}{2}}}$$

$$\boldsymbol{IOA = 1 - \frac{\sum_{i=1}^{N}(P_i - O_i)^2}{\sum_{i=1}^{N}(|P_i - \bar{O}| + |O_i - \bar{O}|)^2}}$$

Where $\boldsymbol{P_i}$ and $\boldsymbol{O_i}$ are the predicted and observed pollutant concentrations, respectively. *N* is

the total number of the predictions used for comparisons, and $\overline{\boldsymbol{P}}$ and $\overline{\boldsymbol{O}}$ represents the average of the prediction and observation, respectively.

Section S3 Synoptic patterns During the Study Episode

Figure S3 presents the mean geopotential heights with wind fields at 500 hPa from 23 to 28 May 2015. In May, the main part of the subtropical high at 500 hPa is located in the western Pacific, with its ridgeline moving around the south of China (Chang et al., 2000; Sui et al., 2007; Jiang et al., 2011). On 23 May 2015, a shallow trough was located between 120°E and 130°E, with the west-northwest wind prevailing over the NCP and its surroundings (Figure S3a). On 24 and 25 May 2015, the high-level trough intensified and moved to the east, the NCP was located behind the trough, and prevailing northwest winds dominate over the NCP (Figures S4b-c). From 26 to 28 May 2015, another weak trough was formed in the westerly wind zone and gradually intensified, moving from 120°E to 130°E. In general, during the study episode, the NCP and its surroundings were located behind the trough and northwest and west flows were prevailing across the region.

Figure S4 shows the variations of the daily mean sea level pressure and wind fields from 23 to 28 May 2015. During the study episode, eastern China was influenced by the high pressure whose center was located in the Yellow Sea, which was caused by the high-level trough. With the warm and humid flow induced by the Asian summer monsoon, rainstorms began to occur in the Pearl River Delta and Yangtze River Delta. The air quality in the NCP, NEC, and NWC was barely influenced by the precipitation during the episode. From 23 to 25 May 2015, when the NCP and its surroundings were located behind the high-level trough, most of the NCP and NWC regions were controlled by high pressures centering in the Yellow Sea. The high pressure system was conductive to the accumulation of air pollutants, increasing the O_3 and $PM_{2.5}$ levels in the NCP. Meanwhile, the low pressure system was

stationed on the north of China. The Liaoning and Jilin provinces were located in the foreside of the low pressure system, and the prevailing southwest wind facilitated the transport of air pollutants from southwest to northeast. From 26 to 28 May, with the eastward movement of the high-level trough, the surface high pressure weather system began to be stagnant over eastern China, and most of the NCP regions were sandwiched between the high pressure located over the Yellow Sea and the deep low pressure lying in the north-south direction across Inner Mongolia and southern China. The resultant prevailing southeast and southwest winds were favorable for the air pollutants transport from the NCP to the NWC and NEC. In summary, under the effects of the low pressure in the continent and the high pressure over the Yellow Sea, the prevailing southeast or southwest winds over the NCP and its surroundings are expected to transport air pollutants from the NCP to the NEC and NWC.

Section S4 Model Evaluation

Section S4.1 Meteorological field simulations

Considering that the meteorological conditions play an important role in the dispersion or accumulation of air pollutants, simulated meteorological fields are compared to the observations. Figure S6 shows the temporal profiles of the simulated and observed surface temperature in the observation sites in Beijing, Tianjin, Shijiazhuang, Shanghai, and Hefei from 22 to 28 May 2015. The WRF-CHEM model generally reproduces the temporal variation of the temperature during the study episode compared with the observations, with *IOA*s exceeding 0.65, but slightly underestimates the temperature in Shanghai and Hefei, particularly during the noontime, with *MB*s of -1.4 and -1.8 °C, respectively. The overestimation of temperature exists in Beijing, Tianjin, and Shijiazhuang, with *MB*s of 3.3, 1.9, and 3.1 °C, respectively. Figure S7 presents the temporal profiles of the simulated and observed surface wind speed in the observation sites in Beijing, Tianjin, Shijiazhuang,

Shanghai, and Hefei from 22 to 28 May 2015. In general, the model performs reasonably in predicting the temporal variation of the wind speed in these cities, particularly in Tianjin, with *IOA* of 0.64, but the simulated surface wind speed is still biased considerably due to the implication of building distributions and heights and the inability of the model for microscale simulations (Chen et al., 2011; Lee et al., 2011).

Section S4.2 Evaluations of $PM_{2.5}$, O_3 and NO_2 Simulations in Northern China

The model generally reproduces the variations of $PM_{2.5}$, O_3 and NO_2 concentrations in Northern China, but the model biases still exist. To further evaluate the model performance, Table S1 shows the statistical comparisons of simulated and measured $PM_{2.5}$ concentrations of 13 provinces over NCP, NEC and NWC of China. Over the NCP, the model simulations in Hebei, Henan and Shandong are much better than the other provinces, with IOA_s of 0.87, 0.80 and 0.85, respectively. The obvious overestimations of $PM_{2.5}$ concentration occur in Beijing, Tianjin and Jiangsu, with *MB* of 10.3 μg m^{-3}, 10.7 μg m^{-3} and 10.4 μg m^{-3}, respectively. The model bias in Beijing is likely attributed to the trans-boundary transport (Wu et al., 2017). The overestimation in Tianjin and Jiangsu might be caused by the marine cloud and the convections, which can not be well resolved in the WRF-CHEM model simulations. The underestimation generally occurs in Anhui province, particular during the last three days, which is perhaps caused by uncertainties of the biomass burning emission. Over the NEC, the $PM_{2.5}$ concentrations in the four provinces are generally influenced by the trans-boundary transport from the NCP when southerly winds are prevailing. So the uncertainties of wind field simulations are one of the most important reasons for the model biases in modeling $PM_{2.5}$ concentrations in the NEC (Bei et al., 2010, 2016a, b). The model performs well in simulating the $PM_{2.5}$ concentration in Shanxi province in the NWC, with *IOA* and *MB* of 0.87 and -1.5 μg m^{-3}, respectively, but the overestimation occurs in Shaanxi province, with *IOA* and *MB* of 0.61 and 8.2 μg m^{-3}, possibly caused by the uncertainty of wind field simulations

and the emission inventory.

Table S2 shows the statistical comparison of simulated and observed O_3 concentrations of 13 provinces in Northern China. The IOA_s of 7 provinces in the NCP are generally more than 0.90, except the Anhui Province, indicating the good model performance in the NCP, but the model is subject to underestimation, particular in Beijing which is influenced by the trans-boundary transport. The model simulation of O_3 concentrations in the NEC is not as good as that in the NCP, and the underestimation is considerable in Jilin, Liaoning and Inner Mongolia, which is plausibly caused by uncertainties of the trans-boundary transport of air pollutants from the NCP to NEC when the southerly wind is prevailing. The O_3 overestimation generally occurs in the NWC, with the *MB* of 7.5 μg m^{-3} and 11.8 μg m^{-3} in Shanxi and Shaanxi provinces, respectively. Table S3 provides the statistical comparison of simulated and observed NO_2 concentrations of 13 provinces in Northern China. The model simulations in Tianjin and Liaoning province are not very good in comparison with the other provinces, with the *IOA*s less than 0.50.

In general, the model can reasonably simulate the variation of air pollutants during the study episode, providing the basis to further investigate the effect of trans-boundary transport of the NCP emissions on the air quality in its surrounding provinces.

Section S5 Effect of interactions between NCP and non-NCP emissions on the Air Quality in the NCP, NEC and NWC

Table S4 summarizes the contribution of interactions between NCP and non-NCP emissions to the daily average $PM_{2.5}$ concentration in the NCP, NEC and NWC from 22 to 28 May 2015. The interaction between NCP and non-NCP emissions generally increases the $PM_{2.5}$ concentration due to the enhancement of precursors of air pollutants and the aerosol radiation feedback. The average contribution of interactions between NCP and non-NCP emissions to the $PM_{2.5}$ concentration in the NCP, Jilin, Liaoning, Shanxi, Shaanxi and Inner

Mongolia is 3.0, 2.6, 7.9, 1.9, 1.7, and 0.8 μg m^{-3}, or 4.6%, 7.5%, 13.3%， 4.4%, 5.5%, and 5.1%, respectively. The contribution of interactions between NCP and non-NCP emissions on the daily afternoon average O_3 concentration in the NCP, NEC and NWC from 22 to 28 May 2015 is summarized in Table S5. On average, the interaction of these two emissions increases the afternoon O_3 concentrations by 16.9, 12.8, 17.9, 12.6, 11.1, and 5.8 μg m^{-3}, or 10.5%, 8.7%, 8.2%, 7.6%, 8.5%, and 5.5%, in the NCP, Jilin, Liaoning, Shanxi, Shaanxi and Inner Mongolia, respectively.

References

Bei, N., Lei, W., Zavala, M., and Molina, L. T.: Ozone predictabilities due to meteorological uncertainties in the Mexico City basin using ensemble forecasts, Atmospheric Chemistry and Physics, 10, 6295-6309, 10.5194/acp-10-6295-2010, 2010.

Bei, N. F., Li, G. H., Huang, R. J., Cao, J. J., Meng, N., Feng, T., Liu, S. X., Zhang, T., Zhang, Q., and Molina, L. T.: Typical synoptic situations and their impacts on the wintertime air pollution in the Guanzhong basin, China, Atmospheric Chemistry and Physics, 16, 7373-7387, 10.5194/acp-16-7373-2016, 2016a.

Bei, N. F., Xiao, B., Meng, N., and Feng, T.: Critical role of meteorological conditions in a persistent haze episode in the Guanzhong basin, China, Science of Total Environment, 550, 273-284, 10.1016/j.scitotenv.2015.12.159, 2016b.

Binkowski, F. S. and Roselle, S. J.: Models-3 Community Multiscale Air Quality (CMAQ) model aerosol component 1. Model description, Journal of Geophysical Research, 108(D6), 4183–18, doi:10.1029/2001JD001409, 2003.

Carnevale, C., Pisoni, E., and Volta, M.: A non-linear analysis to detect the origin of PM10 concentrations in Northern Italy, Science of Total Environment, 409, 182-191, 10.1016/j.scitotenv.2010.09.038, 2010.

Chang, C. P., Zhang, Y., and Li, T.: Interannual and Interdecadal Variations of the East Asian Summer Monsoon and Tropical Pacific SSTs. Part I: Roles of the Subtropical Ridge, Journal of Climate, 13, 4310-4325, 2000.

Chen, F., and Dudhia, J.: Coupling an advanced land surface-hydrology model with the Penn State-NCAR MM5 modeling system. Part I: Model implementation and sensitivity, Monthly Weather Review, 129, 569-585, 10.1175/1520-0493(2001)129<0569:caalsh>2.0.co;2, 2001.

Chen, F., Kusaka, H., Bornstein, R., Ching, J., Grimmond, C. S. B., Grossman-Clarke, S., Loridan, T., Manning, K. W., Martilli, A., Miao, S., Sailor, D., Salamanca, F. P., Taha, H., Tewari, M., Wang, X., Wyszogrodzki, A. A., and Zhang, C.: The integrated WRF/urban modelling system: development, evaluation, and applications to urban environmental problems, International Journal Climatology, 31, 273–288, doi:10.1002/joc.2158, 2011.

Chou, M. D., and Suarez, M. J.: A solar radiation parameterization for atmospheric studies, NASA TM-104606, Nasa Tech.memo, 15, 1999.

Chou, M. D., Suarez, M. J., Liang, X. Z., Yan, M. H., and Cote, C.: A Thermal Infrared Radiation Parameterization for Atmospheric Studies, Max J, 2001.

Gabusi, V., Pisoni, E., and Volta, M.: Factor separation in air quality simulations, Ecological Modelling, 218, 383-392, 10.1016/j.ecolmodel.2008.07.030, 2008.

Guenther, A., Karl, T., Harley, P., Wiedinmyer, C., Palmer, P. I., and Geron, C.: Estimates of global terrestrial isoprene emissions using MEGAN (Model of Emissions of Gases and Aerosols from Nature), Atmospheric Chemistry and Physics, 6, 3181-3210, 2006.

Hong, S.-Y., and Lim, J.-O. J.: The WRF Single-Moment 6-Class Microphysics Scheme (WSM6), Asia-Pacific Journal of Atmospheric Sciences, 42, 129-151, 2006.

Horowitz, L. W., Walters, S., Mauzerall, D. L., Emmons, L. K., Rasch, P. J., Granier, C., Tie,

X. X., Lamarque, J. F., Schultz, M. G., Tyndall, G. S., Orlando, J. J., and Brasseur, G. P.: A global simulation of tropospheric ozone and related tracers: Description and evaluation of MOZART, version 2, Journal of Geophysical Research-Atmospheres, 108, 29, 10.1029/2002jd002853, 2003.

Janjić, Z. I.: Nonsingular Implementation of the Mellor–Yamada Level 2.5 Scheme in the NCEP Meso Model, Ncep Office Note, 436, 2002.

Jiang, X. W., Li, Y. Q., Yang, S., and Wu, R. G.: Interannual and interdecadal variations of the South Asian and western Pacific subtropical highs and their relationships with Asian-Pacific summer climate, Meteorology and Atmospheric Physics, 113, 171-180, 10.1007/s00703-011-0146-8, 2011.

Lee, S.-H., Kim, S.-W., Angevine, W. M., Bianco, L., McKeen, S. A., Senff, C. J., Trainer, M., Tucker, S. C., and Zamora, R. J.: Evaluation of urban surface parameterizations in the WRF model using measurements during the Texas Air Quality Study 2006 field campaign, Atmospheric Chemistry and Physics, 11, 2127–2143, doi:10.5194/acp-11-2127-2011, 2011.

Li, G. H., Zhang, R. Y., Fan, J. W., and Tie, X. X.: Impacts of black carbon aerosol on photolysis and ozone, Journal of Geophysical Research-Atmospheres, 110, 10, 10.1029/2005jd005898, 2005.

Li, G., Lei, W., Zavala, M., Volkamer, R., Dusanter, S., Stevens, P., and Molina, L. T.: Impacts of HONO sources on the photochemistry in Mexico City during the MCMA-2006/MILAGO Campaign, Atmospheric Chemistry and Physics, 10, 6551-6567, 10.5194/acp-10-6551-2010, 2010.

Li, G., Bei, N., Tie, X., and Molina, L. T.: Aerosol effects on the photochemistry in Mexico City during MCMA-2006/MILAGRO campaign, Atmospheric Chemistry and Physics, 11, 5169-5182, 10.5194/acp-11-5169-2011, 2011a.

Li, G., Zavala, M., Lei, W., Tsimpidi, A. P., Karydis, V. A., Pandis, S. N., agaratna, M. R., and Molina, L. T.: Simulations of organic aerosol concentrations in Mexico City using the WRF-CHEM model during the MCMA-2006/MILAGRO campaign, Atmospheric Chemistry and Physics, 11, 3789-3809, 10.5194/acp-11-3789-2011, 2011b.

Li, G. H., Bei, N. F., Zavala, M., and Molina, L. T.: Ozone formation along the California Mexican border region during Cal-Mex 2010 field campaign, Atmospheric Environment, 88, 370-389, 10.1016/j.atmosenv.2013.11.067, 2014a.

Stein, U., and Alpert, P.: Factor separation in numerical simulations, Journal of the Atmospheric Science, 50, 2107-2115, 10.1175/1520-0469(1993) 050<2107:fsins>2.0.co;2, 1993.

Sui, C. H., Chung, P. H., and Li, T.: Interannual and interdecadal variability of the summertime western North Pacific subtropical high, Geophysical Research Letters, 34, 6, 10.1029/2006gl029204, 2007.

Weinhold, B.: Ozone nation - EPA standard panned by the people, Environmental Health Perspectives, 116, A302-A305, 2008.

Wesely, M. L.: Parameterization of surface resistances to gaseous dry deposition in regional-scale numerical models, Atmospheric Environment, 23, 1293-1304, 10.1016/0004-6981(89)90153-4, 1989.

Wu, J., Li, G., Cao, J., Bei, N., Wang, Y., Feng, T., Huang, R., Liu, S., Zhang, Q., and Tie, X.: Contributions of trans-boundary transport to summertime air quality in Beijing, China, Atmospheric Chemistry and Physics, 17, 1-46, 2017.

Zhang, Q., Streets, D. G., Carmichael, G. R., He, K. B., Huo, H., Kannari, A., Klimont, Z., Park, I. S., Reddy, S., Fu, J. S., Chen, D., Duan, L., Lei, Y., Wang, L. T., and Yao, Z. L.: Asian emissions in 2006 for the NASA INTEX-B mission, Atmospheric Chemistry and Physics, 9, 5131-5153, 2009.

279

280 Table S1. Statistical comparison of simulated and measured $PM_{2.5}$ concentrations in the NCP,
281 NEC and NWC.
282

Region	Province	*MB* (μg m^{-3})	*RMSE* (μg m^{-3})	*IOA*
NCP	Beijing	10.3	30.5	0.71
	Tianjin	10.7	33.3	0.52
	Hebei	7.5	14.4	0.87
	Shandong	-1.7	11.7	0.85
	Henan	2.3	21.5	0.80
	Jiangsu	10.4	18.9	0.44
	Anhui	-6.3	22.8	0.43
NEC	Liaoning	-1.5	12.6	0.67
	Jilin	-0.8	12.3	0.58
NWC	Shanxi	-1.5	14.8	0.87
	Shaanxi	8.2	14.6	0.61
NEC+NWC	Inner Mongolia	-11.5	15.4	0.60

283
284

Table S2. Statistical comparison of simulated and measured O_3 concentrations in the NCP, NEC and NWC.

Region	Province	*MB* (μg m^{-3})	*RMSE* (μg m^{-3})	*IOA*
NCP	Beijing	-18.6	46.0	0.90
	Tianjin	-13.6	33.3	0.90
	Hebei	-8.8	19.5	0.96
	Shandong	-14.4	22.5	0.94
	Henan	7.9	23.8	0.94
	Jiangsu	1.3	20.6	0.95
	Anhui	-6.3	22.8	0.84
NEC	Liaoning	-25.4	32.8	0.84
	Jilin	-23.2	34.8	0.83
NWC	Shanxi	7.5	21.3	0.94
	Shaanxi	11.8	23.3	0.89
NEC+NWC	Inner Mongolia	-13.7	19.3	0.92

293 Table S3. Statistical comparison of simulated and measured NO_2 concentrations in the NCP,
294 NEC and NWC.
295

Region	Province	*MB* (μg m^{-3})	*RMSE* (μg m^{-3})	*IOA*
NCP	Beijing	5.0	17.7	0.66
	Tianjin	2.1	20.4	0.31
	Hebei	0.7	12.3	0.67
	Shandong	-0.5	12.3	0.71
	Henan	4.2	13.0	0.74
	Jiangsu	2.7	10.3	0.59
	Anhui	0.4	11.2	0.56
NEC	Liaoning	-0.8	12.7	0.45
	Jilin	3.3	12.2	0.68
NWC	Shanxi	1.7	11.5	0.79
	Shaanxi	4.7	11.1	0.75
NEC+NWC	Inner Mongolia	1.1	7.6	0.88

296
297
298

299 Table S4. Daily average $PM_{2.5}$ contributions (μg m^{-3}) in the NEC, NWC and NCP due to the
300 interaction between NCP and non-NCP emissions from 22 to 28 May 2015.
301

Date	NCP	Jilin	Liaoning	Shanxi	Shaanxi	Inner Mongolia
22	0.02	0.4	1.4	0.07	0.02	0.06
23	1.3	2.4	4.8	1.7	0.2	0.4
24	2.1	3.0	5.6	3.4	0.9	0.6
25	3.2	3.3	8.1	3.0	1.2	1.0
26	5.0	1.1	8.1	1.6	1.9	0.8
27	4.9	1.3	15.6	1.9	3.3	0.7
28	4.7	6.4	11.5	1.8	4.7	2.1
Average (μg m^{-3})	3.0	2.6	7.9	1.9	1.7	0.8
Average (%)	4.6	7.5	13.3	4.4	5.5	5.1

302
303
304

Table S5. Daily afternoon (12:00-18:00 BJT) average O_3 contributions (μg m^{-3}) in the NEC, NWC and NCP due to the interaction between NCP and non-NCP emissions from 22 to 28 May 2015.

Date	NCP	Jilin	Liaoning	Shanxi	Shaanxi	Inner Mongolia
22	12.8	11.6	13.8	11.6	7.3	2.8
23	21.5	16.0	20.1	18.2	12.2	4.6
24	19.6	18.3	21.5	16.2	13.7	7.2
25	20.7	19.4	19.4	14.2	11.7	8.2
26	11.1	10.6	14.9	7.0	10.5	7.3
27	15.6	3.2	17.0	11.1	13.4	5.4
28	17.1	10.8	18.9	9.8	9.1	5.2
Average (μg m^{-3})	16.9	12.8	17.9	12.6	11.1	5.8
Average (%)	10.5	8.7	8.2	7.6	8.5	5.5

Supplement Figure Captions

Figure S1 Defined three sections in Northern China. 1) Northeast China (NEC): Heilongjiang, Jilin, Liaoning, and the east part of Inner Mongolia; 2) Northwest China (NWC): Shanxi, Shaanxi, and the west part of Inner Mongolia; 3) North China Plain (NCP): Beijing, Tianjin, Hebei, Shandong, Henan, and the north part of Jiangsu and Anhui. The red circle marked with number 1 to 5 denotes the meteorological site in Beijing, Tianjin, Shijiazhuang, Shanghai, and Hefei, respectively.

Figure S2 Spatial distribution of anthropogenic emission rates of (a) NO_x, (b) VOC_s, (c) OC, and (d) SO_2 (10^6 g $month^{-1}$) in Mainland China.

Figure S3 Geopotential heights and wind vectors at 500 hPa from 23 to 28 May 2015.

Figure S4 The mean sea level pressure and wind vectors from 23 to 28 May 2015.

Figure S5 Variation of East Asian summer moon index from 1988 to 2017 (Climate Diagnostics and Prediction Division/NCC/CMA).

Figure S6 Comparison of measured (black dots) and predicted (blue line) diurnal profiles of near-surface hourly temperature in Beijing, Jinan, Wuhan, Shanghai, and Zhengzhou from 22 to 28 May 2015.

Figure S7 Comparison of measured (black dots) and predicted (blue line) diurnal profiles of near-surface hourly wind speed in Beijing, Jinan, Wuhan, Shanghai, and Zhengzhou from 22 to 28 May 2015.

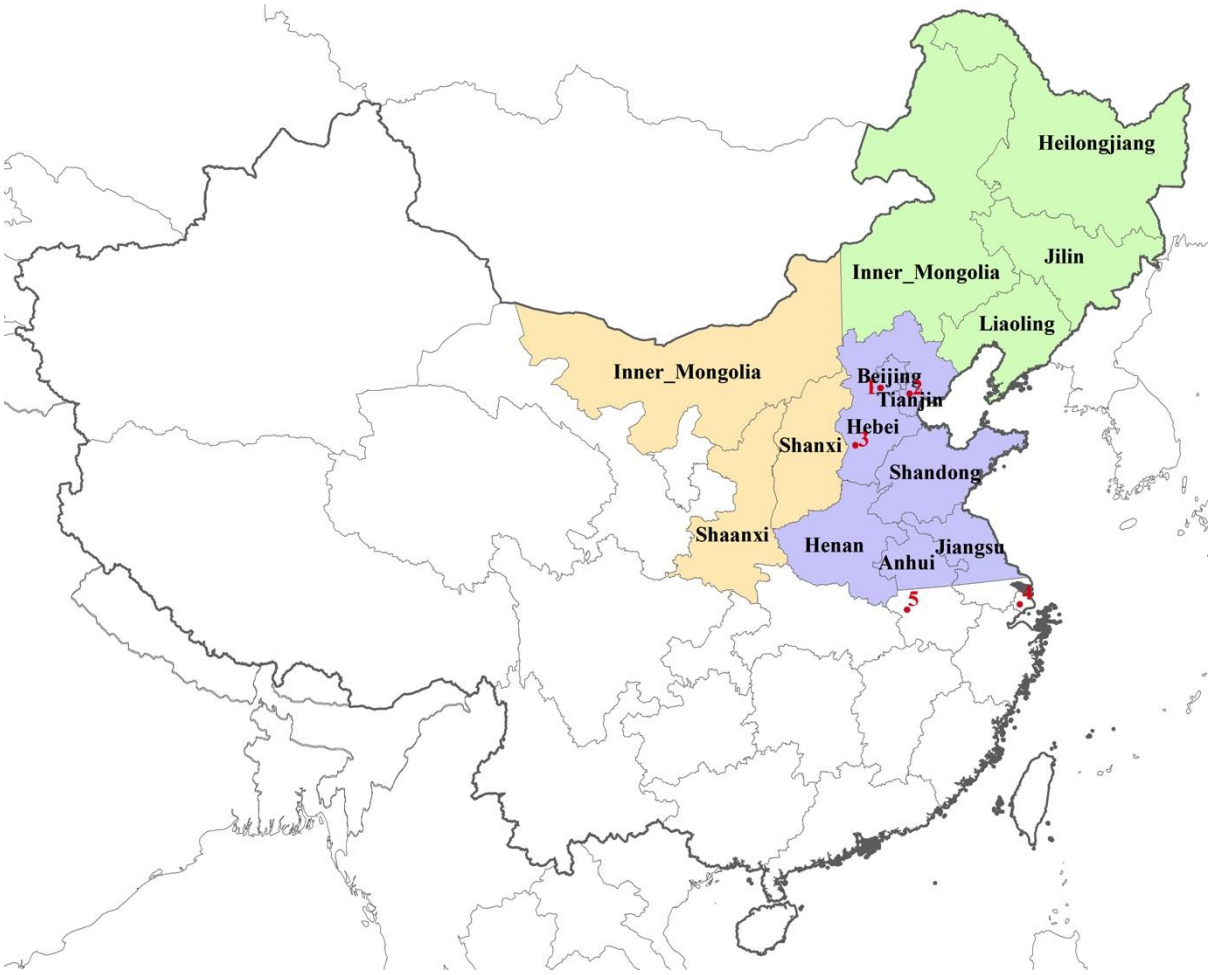

Figure S1 Defined three sections in Northern China. 1) Northeast China (NEC): Heilongjiang, Jilin, Liaoning, and the east part of Inner Mongolia; 2) Northwest China (NWC): Shanxi, Shaanxi, and the west part of Inner Mongolia; 3) North China Plain (NCP): Beijing, Tianjin, Hebei, Shandong, Henan, and the north part of Jiangsu and Anhui. The red circle marked with number 1 to 5 denotes the meteorological site in Beijing, Tianjin, Shijiazhuang, Shanghai, and Hefei, respectively.

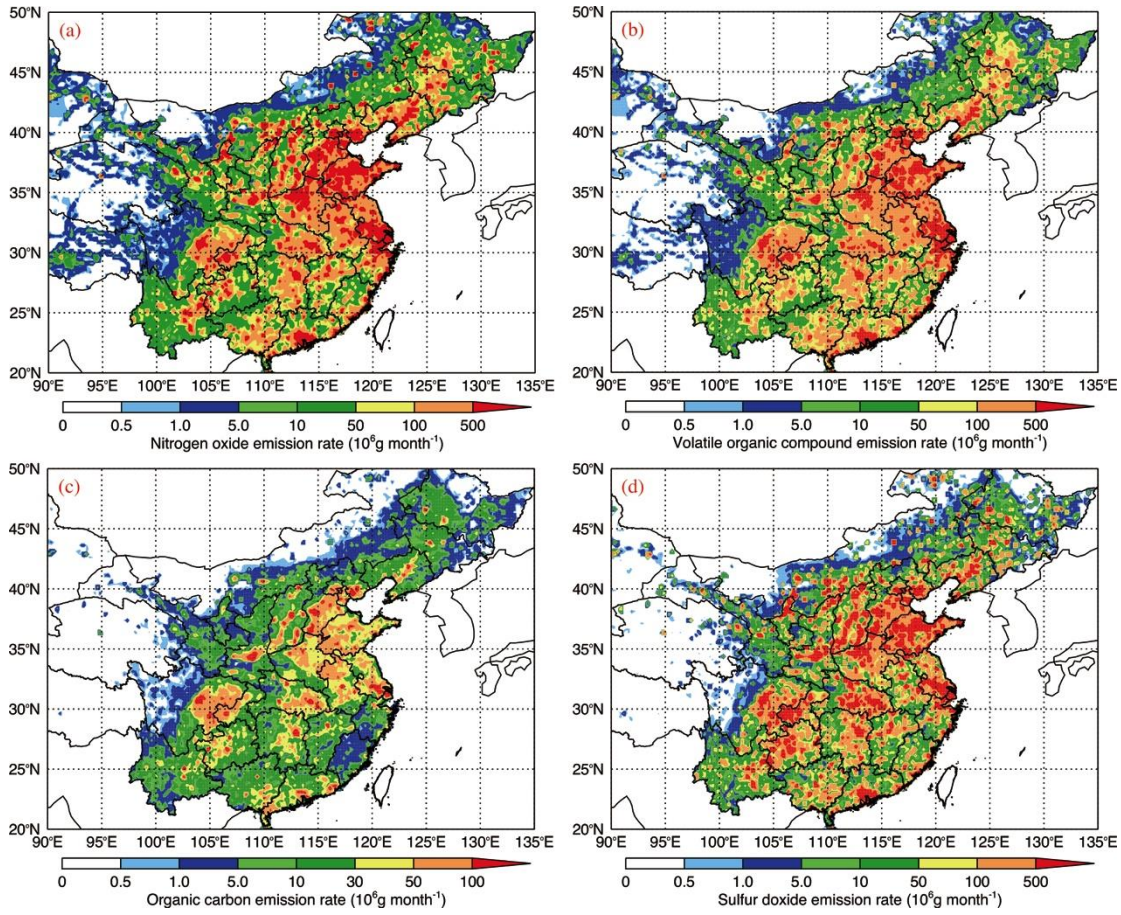

Figure S2 Spatial distribution of anthropogenic emission rates of (a) NO_x, (b) VOC_s, (c) OC, and (d) SO_2 (10^6 g month^{-1}) in Mainland China.

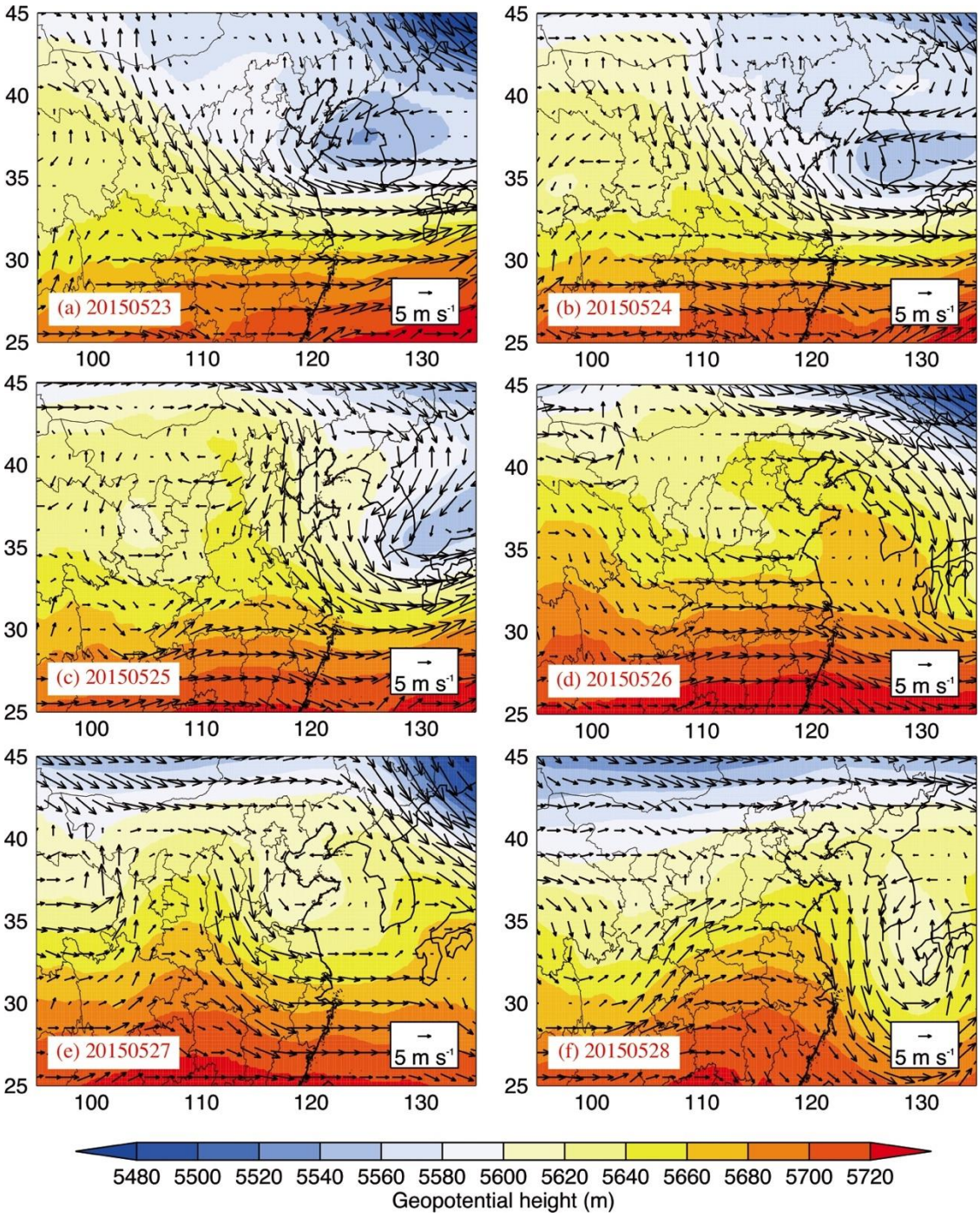

Figure S3 Geopotential heights and wind vectors at 500 hPa from 23 to 28 May 2015.

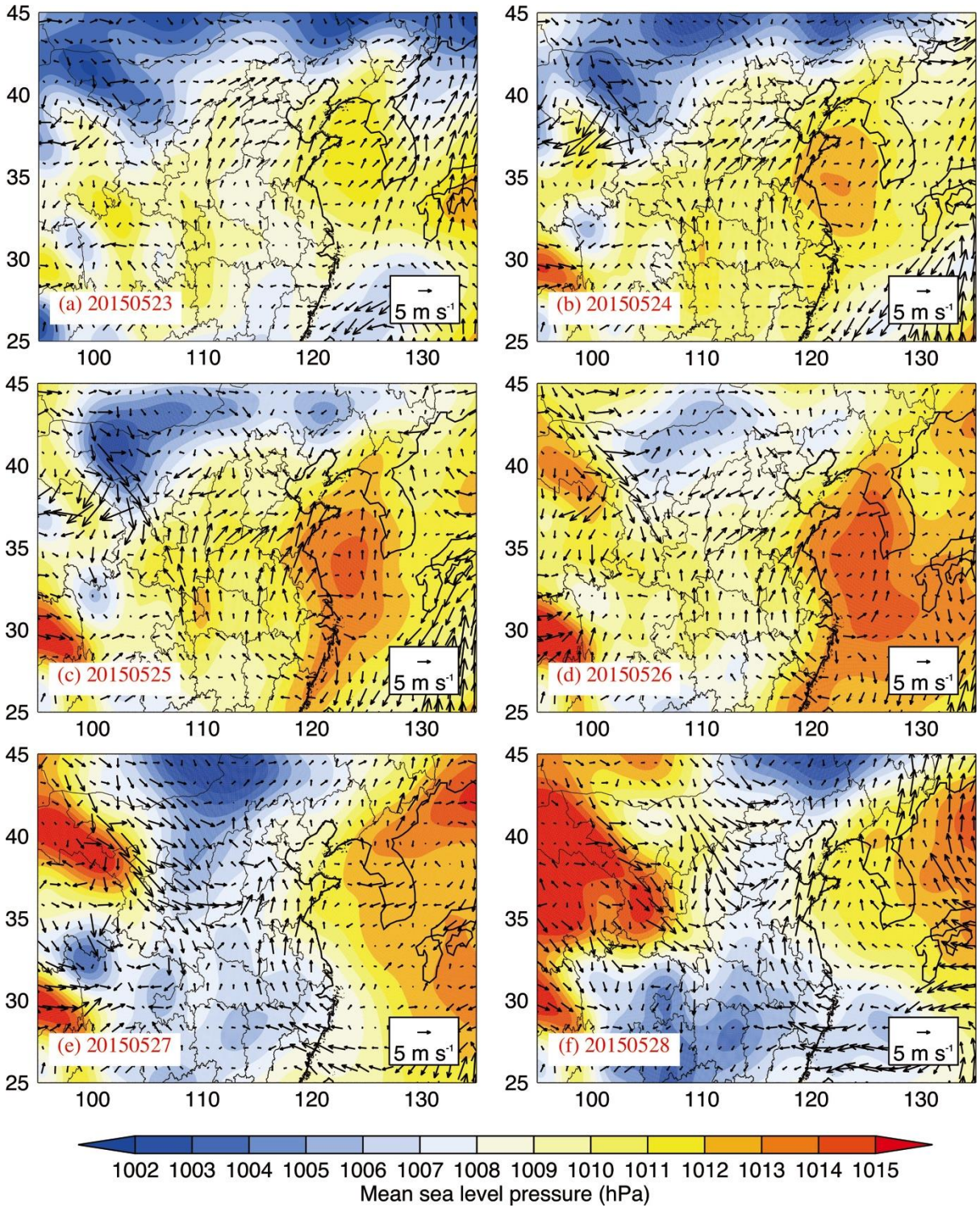

Figure S4 The mean sea level pressure and wind vectors from 23 to 28 May 2015.

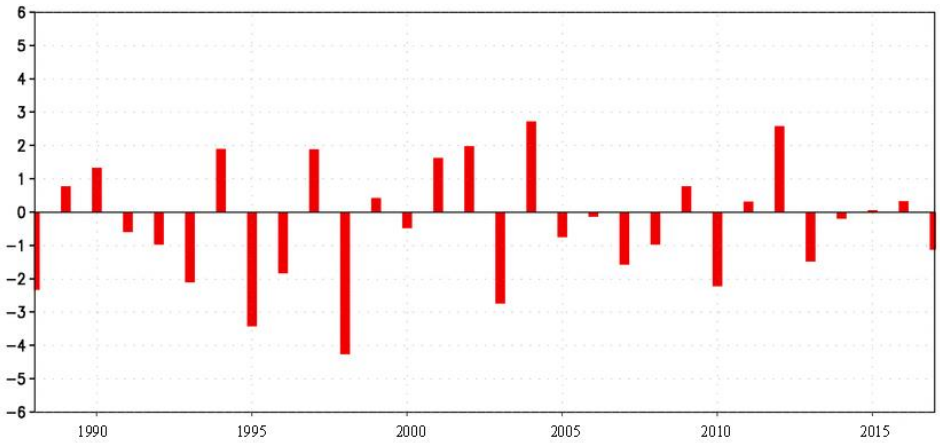

Figure S5 Variation of East Asian summer moon index from 1988 to 2017 (Climate Diagnostics and Prediction Division/National Climate Center/China Meteorological Administration).

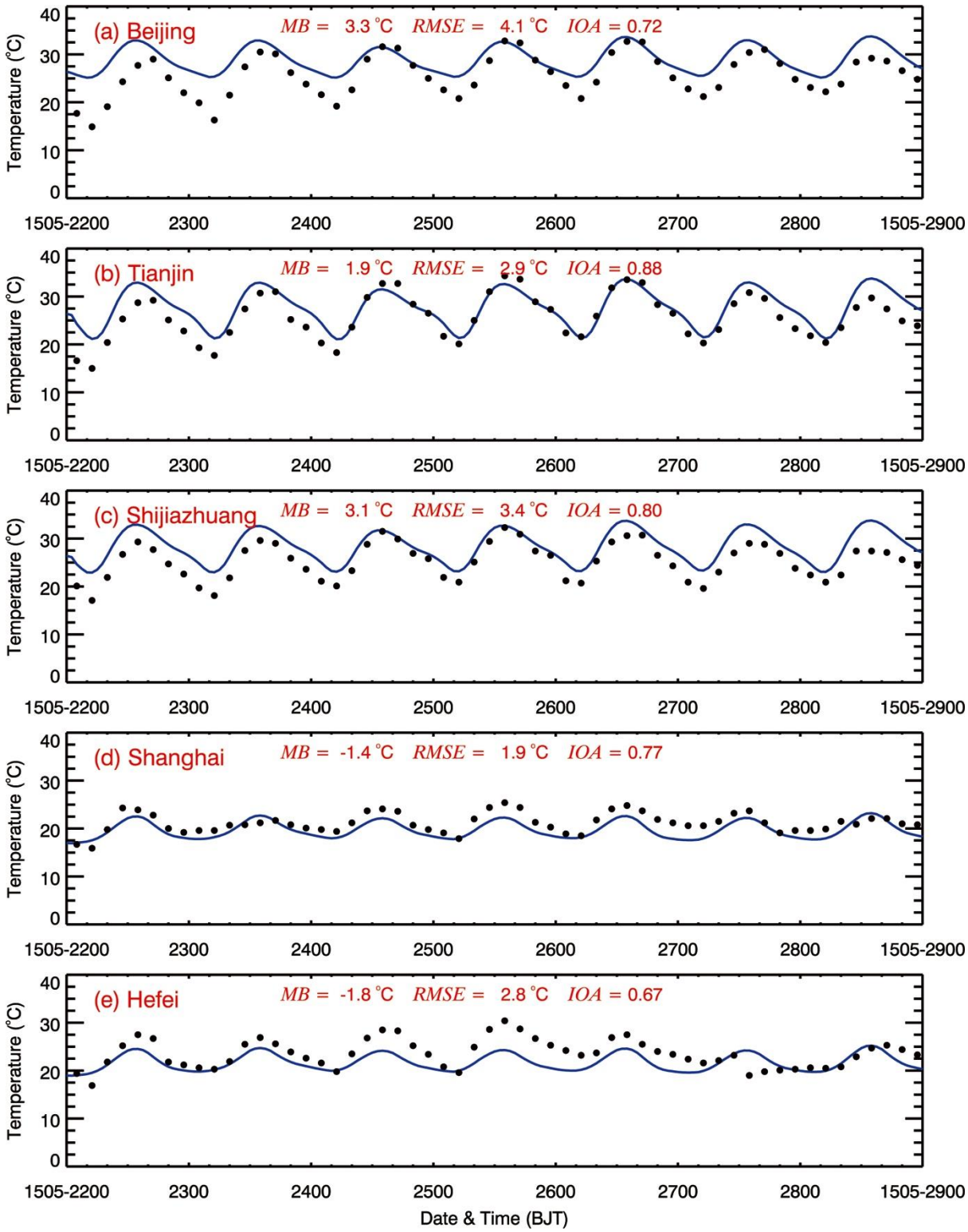

Figure S6 Comparison of measured (black dots) and predicted (blue line) diurnal profiles of near-surface hourly temperature in Beijing, Tianjin, Shijiazhuang, Shanghai, and Hefei from 22 to 28 May 2015.

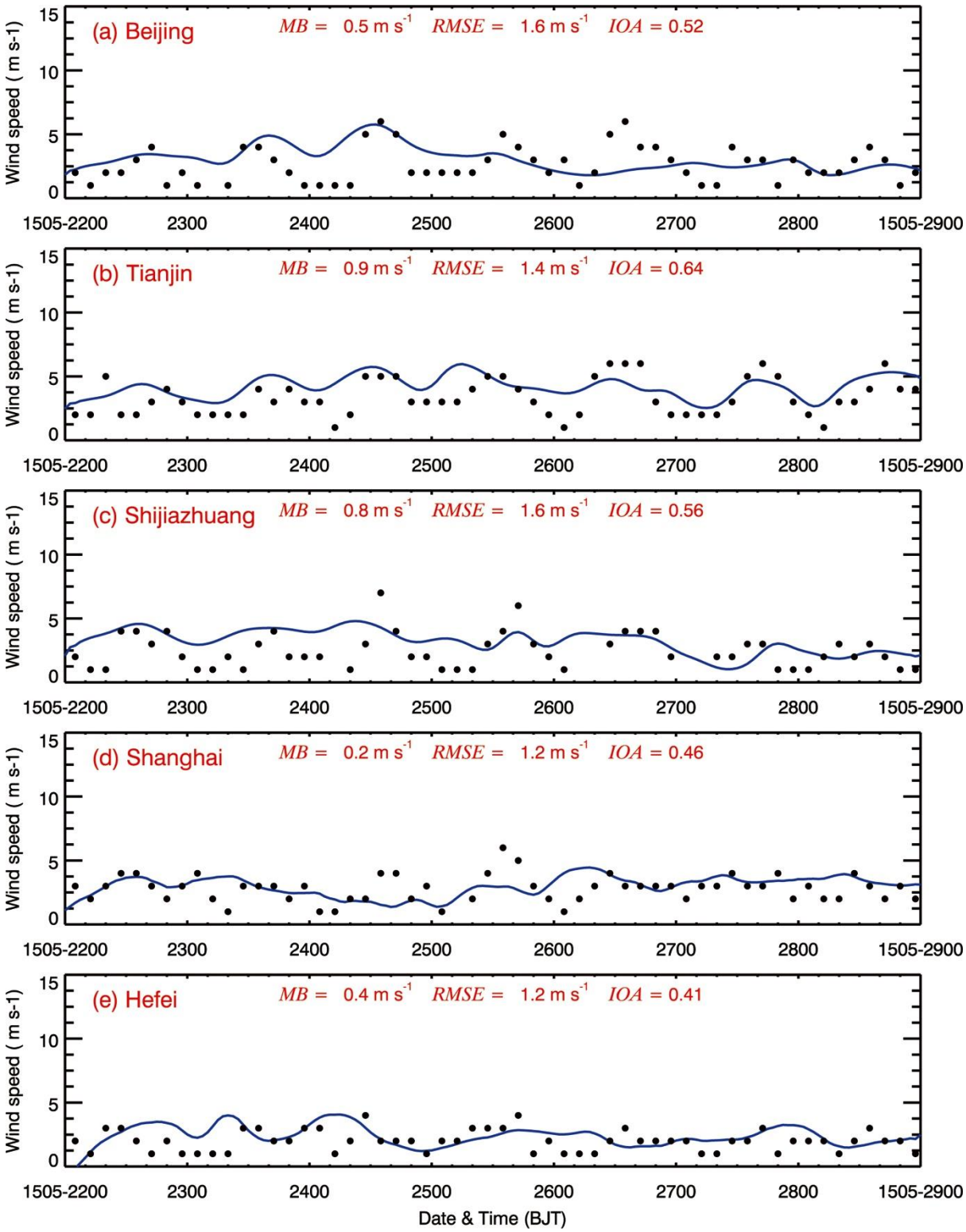

Figure S7 Comparison of measured (black dots) and predicted (blue line) diurnal profiles of near-surface hourly wind speed in Beijing, Tianjin, Shijiazhuang, Shanghai, and Hefei from 22 to 28 May 2015.